

Monday 9-12
Go Forth and Measure Project

Measuring the Heat Absorption and Retention Properties of a Solar Autoclave

5/14/10
2.671 Measurement and Instrumentation

Abstract

Rural health clinics often struggle to sterilize instruments due to a lack of effective sterilization methods. A possible solution is steam sterilization within a solar autoclave, prompting research on the effectiveness and possible improvements to an existing model. This experiment examines the energy absorption, retention, and loss through model components, comparing results to theoretical models of heat loss and to desired results for sterilization. This model absorbed and retained energy at a rate of 29.9 ± 2.7 W, compared to the net 88.1 ± 21 W needed to sterilize one load of medical instruments. 99.3 ± 5.2 % of heat lost was due to conduction through the bottom and sides, prompting design revision through a reduction of non-heat-absorbing areas.

1. Introduction

A functioning solar powered autoclave, used to sterilize medical instruments, has the potential to save a full day of labor each week for nurses at health outposts in rural Nicaragua. In addition, a solar autoclave may save lives when several patients are in critical need of sterilized operating equipment on the same day. Because many health outposts are located far from other hospitals and not connected to an electrical grid, medical personnel must often travel long distances to adequately sterilize certain instruments, gauze, and other material. If rural health outposts possessed an autoclave that functioned reliably off grid, both time and lives would be saved. In response to this challenge, the organizations Salud del Sol, Mujeres Solares de Totogalpa, and engineering students from the Universidad Nacional de Ingeniería have teamed up to design a functioning solar autoclave.

The current autoclave design features a solar powered oven manufactured by the Mujeres Solares, comprised of a well-insulated box with a double paneled glass lid and an adjustable reflector panel. Inside this solar oven is a six quart Presto Pressure Cooker, an inexpensive brand of pressure cooker readily available in Nicaragua. Developments are under way to determine the effectiveness of this combination for reliably sterilizing materials. In determining what changes the design requires, it is necessary to evaluate the ability of the solar cooker to reach sterilization conditions, as well as determine the ways in which the current system may be losing precious heat.

To measure the modes heat loss of the autoclave, this experiment tracks the system's inner and outer temperature over time. The variation in temperature with time allows for modeling the system as a simple circuit along which heat flows rather than electricity. In this thermodynamic model, a thermal resistor represents each layer of insulating material, as well as each surface along which convection or radiation occurs, the estimated quantity of radiation from the sun provides the system's power input, and power is lost through conduction, convection, and radiation. Net power input is tracked by measuring the temperature of the system over time. Modeled heat losses are compared to this net power input, along with incident solar radiation, to confirm conclusions regarding modes of heat loss based on the model.

2. Description and Thermodynamic Modeling of Solar Autoclaves

2.1. How Autoclaves Work

The essential components of an autoclave are a vessel capable of holding high pressure steam and some type of insulation that prevents the energy used from escaping into the outside environment. Conventional autoclaves typically include a high power oven that is also capable of sustaining high internal pressures; high pressure steam is often then injected into the oven's interior. For the type of autoclave used in this experiment, high pressure steam is created by heating the pressure vessel until a small quantity of water present inside begins to boil. The boiling water creates a large quantity of vapor, which is trapped inside the vessel until the internal pressure reaches 200 kPa. This occurs when the internal temperature has reached 121 degrees Celsius. This temperature and pressure, maintained for a total of 15 minutes, are the conditions required for sterilization of medical instruments according to ¹international sterilization standards.

2.2. How Solar Ovens Work

A solar oven relies on the greenhouse effect, whereby radiation from the sun, primarily in the form of visible light, is trapped within a closed system and converted into thermal energy, or infra-red radiation. This is made possible through the use of glass or plastic, which is permeable to visible light but reflects radiation in the infra-red range. Once visible light has passed through the glass or plastic barrier, it is converted into thermal energy through absorption by a dark object. Dark objects appear dark because they absorb visible light; however, they emit the energy they have absorbed in the form of heat. A solar oven therefore includes both a glass or plastic panel and some type of dark object or surface on the interior for the conversion of light into heat. This creation of heat inside the oven, given appropriate insulation on the exterior, allows the oven's interior to increase in temperature, often quite quickly. The oven may then be used to heat food, boil water, or perform most other activities generally possible in conventional ovens.

2.3. Thermal Model of a Solar Autoclave

The solar autoclave design studied here consists of a pressure cooker placed inside a solar oven. In practice, medical instruments would be placed inside the pressure cooker; thus, their mass must be accounted for in determining the power absorption required to reach sterilization conditions. Sunlight is absorbed through a double-paned glass panel at the top and is converted to heat via the pressure cooker's dark surface. Heat loss is prevented through successive layers of insulation on the sides and bottom of the oven, including insulating fiberboard, sawdust, and plywood. Through the top, heat loss is prevented via an air gap small enough to prevent significant convective effects.

Based on the above design, it is possible to construct a model that uses the thermal resistance of each material and solid-to-fluid interface to thermally characterize the autoclave. This model, depicted visually in Figure 1, illustrates the individual thermal resistances responsible for determining the heat transfer rate through each autoclave surface. Because the air temperatures of the oven and outside environment are measured, rather than surface temperatures of the autoclave, additional thermal resistances due to convection between solid and fluid surfaces must be accounted for. Additionally, the thermal resistance provided by the air gap between two panes of glass at the top of the autoclave is based on the thermal conductivity, rather than the convection constant, of air. This is because the sealed environment and small gap prevent motion of the air enough to limit significant conductive effects. Because

the temperature difference between the outer surface of the autoclave and the ambient air is minimal, effects of thermal radiation can be considered insignificant. They are therefore excluded from the heat transfer model. A thorough mathematical description of the model used is provided in section 2.4.

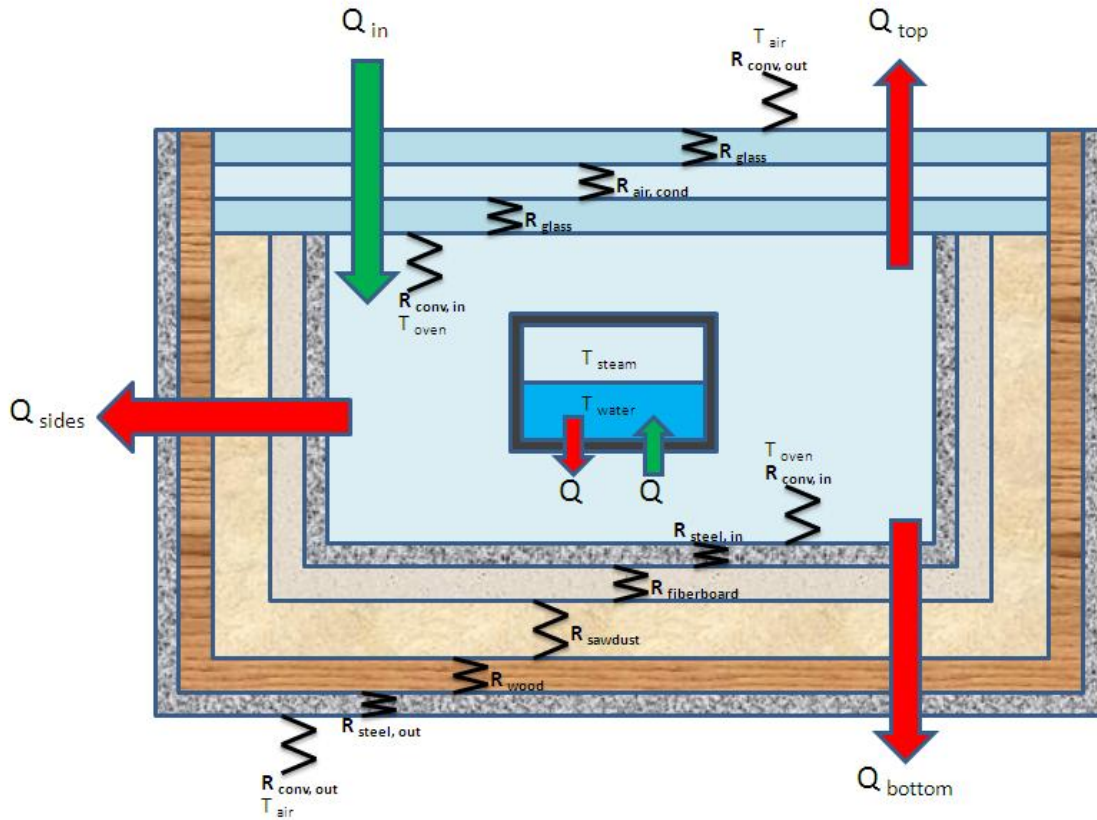


Figure 1: Thermal Model of a Solar Autoclave. The solar autoclave tested consists of a pressure cooker placed inside a solar box cooker. Several layers of insulation are combined to minimize heat loss; each of these layers has a characteristic resistance to heat loss based on its composition, width, and area. Modes of heat loss accounted for in the thermal model include convection at fluid-solid interfaces and conduction through each insulating layer. Resistances at each interface shown are defined according to Equation 10 in section 2.4.

2.4. Mathematical Models of Solar Energy and Heat Transfer

Radiant energy from sunlight is captured through a solar autoclave’s glass paneling. The input power is

$$Q_{in} = I \times A \times \alpha \quad (1)$$

where I is the intensity of the sunlight, and A is the area of the glass panel, and α is the percentage of radiation transmitted through the glass. The light intensity drops to approximately $\frac{1}{3}$ the usual value under light to medium cloud cover².

Equation 1 carries with it specific uncertainty associated with its component variables, the intensity of the sunlight, the percent of the light absorbed, and in particular the measured length and width of the panel absorbing the radiation. Using the uncertainties in these component measurements, it is possible to determine a value for the 95% precision uncertainty of the input power. This is done using the propagation of uncertainty method, shown in Equation 2:

$$u_{Q_{in}} = \sqrt{\left(\frac{\partial Q_{in}}{\partial L} u_L\right)^2 + \left(\frac{\partial Q_{in}}{\partial W} u_W\right)^2}. \quad (2)$$

Here, u_i is the uncertainty in the known value of each variable. Note that the contributions from uncertainty in the value of the intensity of sunlight and the percentage of light absorbed were not included. Although uncertainties in these quantities may not be negligible, it is unknown at this time what the uncertainties are. Uncertainty in the intensity of sunlight is currently unknown from literature and may be added later. Uncertainty in the reflectivity of the particular light absorptive material, such as the window glass used in making a solar autoclave, is here approximated by referencing a chart; the uncertainty is again unknown. Hence, Equation 2 provides a lower bound for the uncertainty in the autoclave's incident power.

The power loss of the system derives from heat loss due to conduction, convection, and radiation to the surrounding environment, summed in Equation 3.

$$Q_{out} = Q_{cond} + Q_{conv} + Q_{rad} \quad (3)$$

Although heat loss through radiation, Q_{rad} , is small enough to be negligible for the system of the solar autoclave, heat loss through conduction and convection, Q_{cond} and Q_{conv} are similarly dependent on the temperature gradient and thermal resistances across surfaces, as shown in Equations 4 and 5.

$$Q_{cond} = \sum \frac{\Delta T}{R_{cond}} \quad (4)$$

$$Q_{conv} = \sum \frac{\Delta T}{R_{conv}} \quad (5)$$

The thermal resistances related to conduction and convection, however, differ in their dependent variables. The thermal resistance through a conducting material is directly proportional to the length L through which heat transfers, and inversely proportional both to the area of the heat transfer, A , and the conduction coefficient, k . This is illustrated in Equation 6. Thermal resistance to convection, however, depends entirely on the area and the convection coefficient, h , shown in Equation 7.

$$R_{cond} = \frac{L}{kA} \quad (6)$$

$$R_{conv} = \frac{1}{hA} \quad (7)$$

When characterizing a thermal system, it is crucial to add the resistances as they would be added for an electrical circuit, shown in Equation 8. Adding resistors in series increases the resistance of a system.

$$R_{series} = R_1 + R_2 + R_3 + \dots \quad (8)$$

It is possible to combine Equations 3 through 8 in order to obtain values for heat loss through all surfaces of the solar autoclave. The air in the oven loses heat through convection to the inner surfaces, then through conduction and convection to the outside air. The total predicted heat loss is

$$\begin{aligned} Q_{out} &= Q_{top} + Q_{sides} + Q_{bottom} \\ &= \frac{\Delta T_{in,out}}{\sum R_{top}} + \frac{\Delta T_{in,out}}{\sum R_{sides}} + \frac{\Delta T_{in,out}}{\sum R_{bottom}}, \end{aligned} \quad (9)$$

where the heat loss through the top, bottom, and sides is determined by the temperature difference between the oven and the environment, $\Delta T_{in,out}$, and the thermal resistance over the surface, $\sum R$. For each surface, the total resistance is

$$\begin{aligned} \sum R &= R_{conv,oven} + \sum R_{cond,materials} + R_{conv,outer} \\ &= \frac{1}{h_{oven} \times A_{inner}} + \sum \frac{L_{ins}}{K_{ins} \times A_{ins}} + \frac{1}{h_{outer} \times A_{outer}}, \end{aligned} \quad (10)$$

where h is the convection coefficient³ in for air in each location, L and K are the thickness and conduction coefficient⁴ of each insulation material, and A is the area of the inner and outer surfaces of the cooker. For details on the conduction and convection coefficients used in determining the thermal resistance each material and fluid/solid boundary, see Appendix A.

Equations 9 and 10 carry with them many sources of uncertainty, which can be combined to determine the 95% precision uncertainty in the solar autoclave's power loss. This is done through the propagation of uncertainty method as discussed previously in relation to Equation 2. The resulting uncertainty in Q_{out} is

$$u_{Q_{out}} = \sqrt{\sum \left(\frac{\partial Q_{out}}{\partial \Delta T_{in,out}} u_{\Delta T_{in,out}} \right)^2 + \sum \left(\frac{\partial Q_{out}}{\partial L} u_L \right)^2 + \sum \left(\frac{\partial Q_{out}}{\partial A} u_A \right)^2 + \sum \left(\frac{\partial Q_{out}}{\partial h} u_h \right)^2}, \quad (11)$$

where u_i is the uncertainty inherent in each variable listed. Note that uncertainties in the conduction coefficients were not included since standard values for these were used, as recorded in Appendix A.

Energy absorption is tracked through temperature increases and phase changes. For this system, the predicted change in energy is

$$\Delta E = E_{in} - E_{out} = \sum_{materials} \int mc \frac{dT}{dt} + m_{\Delta phase} \times H_{vap}, \quad (12)$$

where m , c , and $\frac{dT}{dt}$ are the mass, specific heat, and temperature change (with time) of each material heated. H_{vap} is the heat of vaporization of water⁵, equal to 2.261 J/kgK, while $m_{\Delta phase}$ is the amount that changed to steam.

For systems in which no material changes phase, Equation 12 can be simplified to exclude the second term. This makes it easy to differentiate the equation with respect to time, thus obtaining the net power input for the system, shown in Equation 13.

$$Q_{net} = \sum_{materials} mc \frac{dT}{dt}, \quad (13)$$

where $\frac{dT}{dt}$ is the slope of the graph depicting each material's increase in temperature with time. Precision uncertainty in the measurement of net power input can be calculated through a combination of the propagation of uncertainty method and the computation of uncertainty in the slope of $\frac{dT}{dt}$. The uncertainty in the slope of $\frac{dT}{dt}$ can be determined through the aid of several different graphing and analysis programs; however, Equations 14 through 16 in the Experimental Setup section describe exactly how the uncertainty was calculated in this experiment.

2.5. Determining the Autoclave's Required Power Absorption

It is also possible to determine the minimum amount of power absorption the tested autoclave would need to sterilize medical instruments. To be functionally competitive with electrical and gas powered autoclaves, a solar autoclave should ideally be able to heat one load of medical instruments to sterilization temperatures within 45 minutes¹. A standard, complete kit of steel surgical instruments⁶ weighs approximately 1.4 kg. Filling the pressure vessel with steam⁷ at sterilization pressure and accounting for typical losses⁸ requires only 6.7 grams of water. The net power required to heat the steel instruments, water, and aluminum pressure vessel can therefore be approximated as

$$Q_{requ} = \frac{\Delta E}{\Delta t} = \frac{(m_i c_i \Delta T_i + m_{pc} c_{pc} \Delta T_{pc} + m_w c_w \Delta T_w + m_s c_s \Delta T_s) + m_w H_{vap}}{\Delta t}, \quad (14)$$

where Δt is the desired 45 minute¹ heating time, m_i is the mass of the medical instruments, m_{pc} is the mass of the pressure cooker, m_w is the mass of the water required to fill the pressure vessel with steam, and m_s , the mass of the steam, is equal to m_w . Each c is the material's accompanying specific heat capacity, while the accompanying ΔT is the temperature change that material must undergo. For details on the specific heat of each material modeled⁹, see Appendix A. Note that the medical instruments and pressure cooker must undergo a temperature change of approximately 100° C, while the water must increase its temperature by 79° C to boil. The steam then requires a further 21° C increase to reach sterilization temperature. The starting temperature

for the system is based on an average 21° C average daytime outdoor temperature in Managua. H_{vap} is the heat of vaporization of water.

The largest source of uncertainty in Equation 14 is by far the change in temperature needed to reach sterilization conditions. While it is modeled based on the average daytime temperature in Managua, in reality the temperature change required will vary depending on the time of year, altitude, how long the cooker has been sitting in the sun, and a variety of other factors. It easily varies by as much as 50° C, providing the following lower bound for the uncertainty in Q_{requ} :

$$u_{Q_{requ}} = \sqrt{\sum \left(\frac{\partial Q_{requ}}{\partial \Delta T_n} u_{\Delta T_n} \right)^2}, \quad (15)$$

where ΔT_n is the total temperature change required by each material mentioned in equation 14. The sum therefore includes ΔT_i , ΔT_{pc} , ΔT_w , ΔT_s . $u_{\Delta T_n}$ refers to the uncertainty in each of these temperature differences, respectively.

3. Measuring the Heat Absorption, Retention, and Modes of Loss

In order to accurately characterize the solar autoclave system, it was necessary to take four temperature measurements of different parts of the system. Measurements taken included the temperature of the water and of the vapor inside the pressure cooker, the air temperature on the interior of the oven, and the air temperature outside the oven. Measuring equipment was carefully placed in the required locations, and then the pressure cooker was inserted into the solar oven. The experimental setup is shown in Figures 2 through 3. Temperature readings were then taken every thirty seconds for two hours. Subsequent to the experiment, data was analyzed through the use of MathCAD to determine the heat transfer rate to each part of the oven. Measurements of various aspects of the system were then incorporated into a thermodynamic model to determine the heat loss of various parts of the system. Afterward, a short follow-up experiment was undertaken to confirm the validity of the approximation used for the thermal resistance of the air gap between the autoclave's two glass panes.

3.1. Preliminary Construction of the Solar Oven

The solar oven was constructed previously by students at the Universidad Nacional de Ingeniería according to instructions provided by Mujeres Solares¹⁰. A large open interior surrounded by several layers of insulation on the sides and bottom. The interior of the oven is lined with galvanized steel to reflect the sunlight. The galvanized steel is encased in a layer of insulating fiber board. Together, these layers form an interior box that is elevated from the base, and connected to the outer box, by several pine supports. The outer box is lined created primarily from plywood and lined on the sides and bottom with galvanized steel. The top of the outer box is created from two layers of window glass sealed with silicone. The space between the inner and outer box is filled with sawdust. The solar cooker also includes a lid, which is coated in a layer of aluminum foil, to reflect more sunlight when the sun is at a low angle. All specific details of the solar oven construction can be found in supporting material provided by Mujeres Solares.

3.2. Pressure Cooker Design

The other primary component of the autoclave is the Presto pressure cooker, a pre-purchased six quart container composed primarily of 1.5 mm thick aluminum. The pressure cooker, as shown in Figure 1, was painted with matte black acrylic paint several weeks prior to the experiment. The pressure cooker also includes a release valve at the top center, which ensures any pressure in excess of 200 kilopascals will be released.

3.3. Placing Temperature Sensors

Two Spectrum model RT24 surface temperature sensors were first placed inside the pressure cooker. The white surface temperature sensor was placed inside the 1 L of water, while the black surface temperature sensor was placed so as to reach toward the center of the pressure cooker to measure vapor pressure. These sensors were held in place as the lid was screwed on, as shown in Figure 2. Removing the lid at the end of the experiment confirmed they had remained in the correct positions. The pressure cooker was then centered at the bottom of the solar oven, as shown in Figure 3.



Figure 2: Surface Temperature Sensors Inside Pressure Vessel. The white surface temperature sensor was immersed in water, while the black surface temperature sensor was suspended in the air to measure the vapor temperature. Temperature sensors were secured in place through friction with the pressure vessel lid.



Figure 3: Pressure Vessel with Temperature Sensors Inside Solar Oven. The pressure vessel, with its surface temperature sensors, was placed in the center of the solar oven. Wires to the surface temperature sensors were passed through the door of the oven, which was then closed. In the back left corner of the solar oven, several inches from the pressure vessel, was an ACURITE brand oven thermometer used to measure the oven's interior air temperature.

An ACURITE model oven thermometer was then placed several inches from the pressure cooker on the left side to measure the ambient air in the oven. Then a Spectrum model ATP general purpose temperature sensor was attached to the front right edge of the metal stand holding the solar oven, away from any possible shadows. The stiffness of its wire kept the temperature probe suspended in the air, measuring the ambient temperature. The two surface temperature sensors and the temperature probe were then connected to digital readouts located at the left side of the solar cooker.

3.4. Taking Temperature Data and Measuring Oven Dimensions

Exactly a liter of water was measured out using a 250 mL beaker. Due to lack of access to digital recording technology, data was taken by hand every 30 seconds, as shown in Figure 4. Recording the output in the field notebook required 15-25 seconds, leaving time to ensure correct recording and note the presence of any clouds or unsuspected temperature variations. Data was taken from approximately 10:45 am to 12:30 am.



Figure 4: Data Recording Procedure. The displays for digitally measured temperatures were placed at the front left of the solar oven. These included the digital display for the two temperature sensors inside the pressure vessel, as well as the display for the ambient temperature. The display for the ambient temperature was linked to a temperature probe placed in direct sunlight at the front right of the solar oven. Displays for the digital readouts and for the analog oven temperature display were read every 30 seconds for approximately two hours. These were recorded by hand, along with notes on any cloud cover, before being digitized.

Outside time spent data recording, detailed measurements were taken of the solar oven. These were performed using a tape measure. The brand of tape measure used, however, is unknown since the label had worn off. The tape measure was used to determine the length and width of all sheets of material used in the solar oven. Thicknesses of materials used, however, were often impossible to measure without disassembling the oven. The thicknesses of these materials were determined by referencing the information provided by Mujeres Solares.

To determine solar masses of system components, the weights of the pressure cooker and solar oven were measured. Since a large scale was not available, the weight of the solar oven was estimated through lifting and subsequent comparison with the weights of other objects. This led to a large uncertainty in the mass of the solar oven; however, the error in estimation happened not to propagate because the oven temperature remained roughly constant throughout the experiment. To determine the mass of the pressure cooker, another pressure cooker of the same size and model was placed on a digital scale used to weigh people. The model number of the scale is unknown since it was not listed on the product; however, the scale was zeroed and determined to weigh accurately in comparison with other scales.

3.5. Determining the Slope of Best Fit of Temperature with Time

To find the slope of water temperature with time, $\frac{dT_{water}}{dt}$, we graphed the resulting temperature change with respect to the time over which the temperature changed. Then we found the line of best fit. The result was a linear slope. $\frac{dT_{water}}{dt}$ is that slope, as discussed in the background. To determine the uncertainty in the resulting value of $\frac{dT_{water}}{dt}$, we used MathCAD to run an uncertainty analysis on the slope of temperature change versus time change. The uncertainty in the slope was determined using Equations 16 through 18.

$$P_{slope} = 2 \times \frac{s}{S} \quad (16)$$

$$s = \sqrt{\frac{\sum (T_{water} - T_{wfit})^2}{n - 2}} \quad (17)$$

$$S = \sqrt{\sum (T_{water} - T_{wmean})^2} \quad (18)$$

In Equation 16, P_{slope} is both the uncertainty in the slope and in the accompanying value of $\frac{dT_{water}}{dt}$. The variables s and S are determined using Equations 16 and 17, respectively.

In Equation 17, T_{water} is the water's measured temperature output, whereas T_{wfit} was the best fitting value of temperature for each point in time plotted. n is the number of data points determined for temperature versus time. We are concerned primarily with the temperature's deviation from the mean for all values, T_{wmean} . The precision uncertainty in the temperature versus time slope obtained from these values was later useful in determining our precision uncertainty in the solar autoclave's measured net power input.

3.6. Key Assumptions for Modeling System

For modeling this system, the following key assumptions were made:

1. The solar radiation is approximately direct, that is, perpendicular to the surface of the solar autoclave. The effect of this approximation is that it becomes unnecessary to figure in the slight effect of the reflector panel, which is somewhat more difficult to model and does not contribute significantly to the amount of incident solar radiation received by the autoclave.
2. The outer surface of the oven is that of the ambient air. The basis for this assumption is simply touching the outer surface and observing that it did not feel hot or cold. Since it was metal, this would only happen at body temperature, which was approximately the same as ambient. The result of this assumption is that no heat loss occurs due to radiation on the outer surface of the autoclave. All heat loss through the top, bottom and sides is then due to conduction and convection as described via the thermal model shown in Figure 1.
3. No heat is lost from the pressure cooker to the oven through convection currents. This assumption is based on the fact that the oven temperature was consistently higher than that of the pressure cooker.
4. The pine supports do not contribute significantly to conduction to the outside air. This assumption made the system much easier to model.

5. The amount of convection occurring between the two layers of glass at the top surface of the autoclave is insignificant, due to the small size of the gap between them. Hence, the thermal conductivity of air was used in calculating the resistance due to the gap. A small follow-up experiment was later conducted to examine this assumption.
6. The thermal mass of the solar autoclave's insulation materials does not contribute to its energy absorption during heating. This is because both the internal oven temperature and the ambient air temperature remain relatively constant over time, indicating the interior temperature of the insulation materials also does not change. The air inside the solar oven also does not contribute significantly to the thermal mass of the system. The result of these assumptions is that only the mass of the pressure cooker and water contribute to the portion system's thermal mass of the system that absorbs energy during measurement.
7. Moderate cloud cover, when present, reduced the intensity of incident sunlight to approximately $\frac{1}{3}$ of its usual value (determined by looking up the value for incident solar radiation in direct sunlight at noon in Managua). The basis for this assumption is that research on solar panels shows 33% panel efficiency during periods of mild to moderate cloud cover.
8. The density of water can be approximated as constant over the temperatures experienced during measurement. The density of water at the average temperature was used, 980 kg/m^3 . This approximation made the calculation of water's heat capacity much easier to perform. The approximation has a negligible effect on the result since water's density changes by only four percent over the entire temperature range investigated.

3.7. Examining the Thermal Resistivity of Small Air Gaps

A follow-up experiment was performed to investigate whether the resistivity of the autoclave's air gap was correctly modeled based on air's heat conductivity rather than its convection coefficient. The experiment was performed by monitoring heat loss through an air gap in two clear glass jars. Although matching glass jars with an air gap no smaller than 15 mm could be found, it was assumed that if convective effects were found to be minimal, as expected from prior research, the thinner air gap present in the autoclave would likewise exhibit limited convective effects.

3.7.1. Construction of Air Gap Experiment

To perform the experiment, an ice cube was placed in a pre-chilled clear spice jar, which was filled the rest of the way with $48 \pm 1 \text{ mL}$ of ice-cold water. (The spice jar was pre-chilled by soaking for five minutes in ice water, which helped keep the jar's temperature constant throughout the experiment, limiting significant heat absorption by the glass.) A Vernier STS surface temperature sensor was taped to the inner edge of the jar using electrical tape. The jar was then sealed and placed upside down in a second clear glass jar. The smaller jar was centered inside the large one, maintaining an air gap of $15.0 \pm 0.05 \text{ mm}$ on all sides except the bottom. The specific glass jars were so chosen because they maintained the smallest available air gap. A stack of paper slips measuring $3 \pm 0.05 \text{ mm}$ in total height was used to create an air gap distance between the tops of the jars which matched the distance between the sides of the jars.

To limit possible conduction through the bottoms of the jars, the outer jar was placed in a saucer of ice water. Ice in the saucer was replenished as necessary through the course of the experiment. This maintained the bottom of the jars at 0° C, the same as that of the inner jar, preventing any possible heat loss through that surface. To monitor the ambient air temperature near the surface of the outer jar, a Vernier TMP-BTA temperature probe was held approximately 3 cm from the edge of the outer jar throughout the course of the experiment. The preliminary experimental setup is shown in Figure 5.



Figure 5: Experimental Setup of Air Gap Experiment. To determine whether air's thermal conductivity may be used to model its resistance to heat transfer for small gaps, the heat transfer rate through two jars was studied. An air gap of 15 ± 0.2 mm was maintained between all glass surfaces. The heat transfer rate was determined by measuring the time necessary to melt a given mass of ice. The heat transfer rate was used in conjunction with the temperature difference between the jars to determine the resistivity of a 15 mm air gap. A temperature probe was held in the air near the experimental setup to monitor the ambient temperature.

3.7.2. Thermal Analysis and Measurement Strategy

The experimental setup was used in conjunction with the heat transfer model shown in Figure 6 to determine the heat conduction coefficient of the air gap between the glasses. The heat transfer rate, Q_{sys} , was approximated as

$$Q_{sys} = \frac{\Delta E_{ice}}{\Delta t} = \frac{m_{ice} H_{fus}}{\Delta t} = \frac{T_{inner} - T_{air}}{R_{glass,in} + R_{gap} + R_{glass,out} + R_{conv,out}} \quad (19)$$

where m_{ice} is the mass of the ice that melted, Δt is the time it took to melt, and H_{fus} is the heat of fusion for ice¹¹, equal to 333.6 J/g. T_{inner} and T_{air} are the inner and outer measured temperatures, respectively. R in each case is the thermal resistance of the material referenced, determined as in Equation 10.

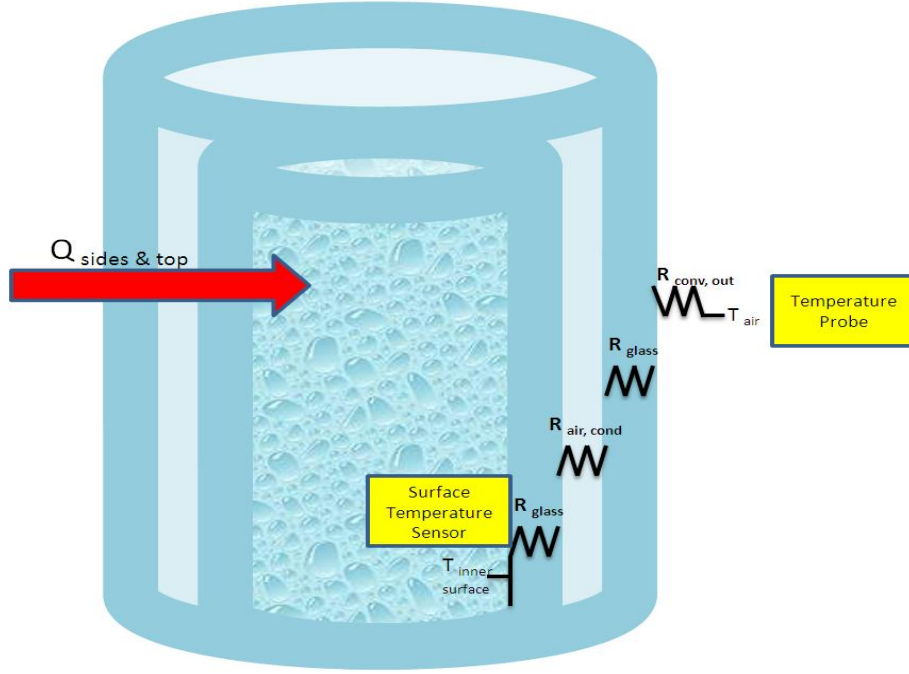


Figure 6: Modeling the Heat Transfer Through the Jars. To determine the resistivity of the air gap between the jars, two temperature sensors were used. A surface temperature sensor measured the inner surface temperature of the small glass, while a temperature probe measured the external air temperature. The heat transfer through the sides and top of the jars was determined by measuring the time required to melt a piece of ice inside the smaller jar. Three of the thermal resistances are known. The last, $R_{air,cond}$, was determined from knowledge of the heat transfer rate, the measured temperature difference, and the other three thermal resistances.

It is possible to combine Equations 10 and 19 to determine the expected conductivity of air in the gap, K_{gap} :

$$K_{gap} = \frac{L_{gap}}{R_{gap}A_{gap}} = \frac{L_{gap}}{\left(\frac{\Delta T}{\frac{m_{ice}H_{fus}}{\Delta t}} - (R_{glass,in} + R_{glass,out} + R_{conv,out}) \right) A_{gap}}, \quad (20)$$

where ΔT is the temperature difference $T_{inner} - T_{air}$ and L_{gap} is the width of the air gap between the glasses.. The uncertainty in the value of K_{gap} is accordingly determined to be

$$u_{K_{gap}} = \sqrt{\sum \left(\frac{\partial K_{gap}}{\partial R_i} u_{R_i} \right)^2 + \left(\frac{\partial K_{gap}}{\partial L_{gap}} u_{L_{gap}} \right)^2 + \left(\frac{\partial K_{gap}}{\partial \Delta T} u_{\Delta T} \right)^2 + \left(\frac{\partial K_{gap}}{\partial A_{gap}} u_{A_{gap}} \right)^2 + \left(\frac{\partial K_{gap}}{\partial \Delta t} u_{\Delta t} \right)^2 + \left(\frac{\partial K_{gap}}{\partial m_{ice}} u_{m_{ice}} \right)^2}, \quad (21)$$

where R_i is the resistance of each of the other interfaces, L_{gap} is the width of the gap, and A_{gap} is its area. Here, u_i is, again, the uncertainty inherent in each variable referenced.

Initial and final volumes of water were measured using a needleless syringe, while the jar thicknesses, diameters, and heights, along with the paper pad height, were measured prior to the experiment using a pair of Vernier calipers. The mass of the ice was determined after melting by subtracting the initial volume of water added to the jar from the total volume of water recorded

after the experiment. Height and diameter measurements were used to determine the spacing between the glass jars. Temperature data from the surface sensor and probe were monitored and recorded using Vernier Logger Pro software. Note that the point at which the ice had fully melted was determined visually, at which point the timer experiment was stopped.

4. Results and Discussion

Theoretically, it would have been possible for the autoclave to absorb 127.7 ± 8.2 W from the sun on the day tested. However, its net power absorption, based on internal temperature increases, was only 29.9 ± 2.7 W. The total power loss was therefore calculated to be 97.8 ± 8.3 W, confidently within the range of the theoretically modeled power loss, 94.88 ± 33 W. The power loss from the top was modeled as 0.667 ± 0.05 W, while the power loss from the sides and bottom of the autoclave were modeled at 59.7 ± 12.7 W and 34.4 ± 12.4 W, respectively. To reach sterilization conditions for one common load of medical instruments within the desired time frame would have required 88.1 ± 21 W of net power absorption. To reach this necessary power requirement, the loss must therefore be reduced by approximately 60 %. Additionally, the upper bound for the heat transfer coefficient for the air gap, as determined from the follow-up experiment, was 0.03 ± 0.008 W/mK. This result contains with 95% confidence the thermal conductivity of air, 0.024 W/mK, indicating it is reasonable to approximate the resistance of the autoclave's air gap as being due to conduction only.

4.1. Autoclave Heating Rate

Recorded temperature data for the ambient air, autoclave oven air temperature, water vapor temperature, and water temperature is shown in Figure 7. The temperature of the water and water vapor slowly reach equilibrium with the oven temperature. The oven temperature, whose average did not increase over time, shows large temporary variation. This can be attributed to the presence of intermittent cloud cover, which was present for 15 ± 1 % of the time the experiment was running. The average slope, or heating rate, of the water inside the pressure cooker was found to be $18.2 \pm 6.2^\circ$ C per hour.

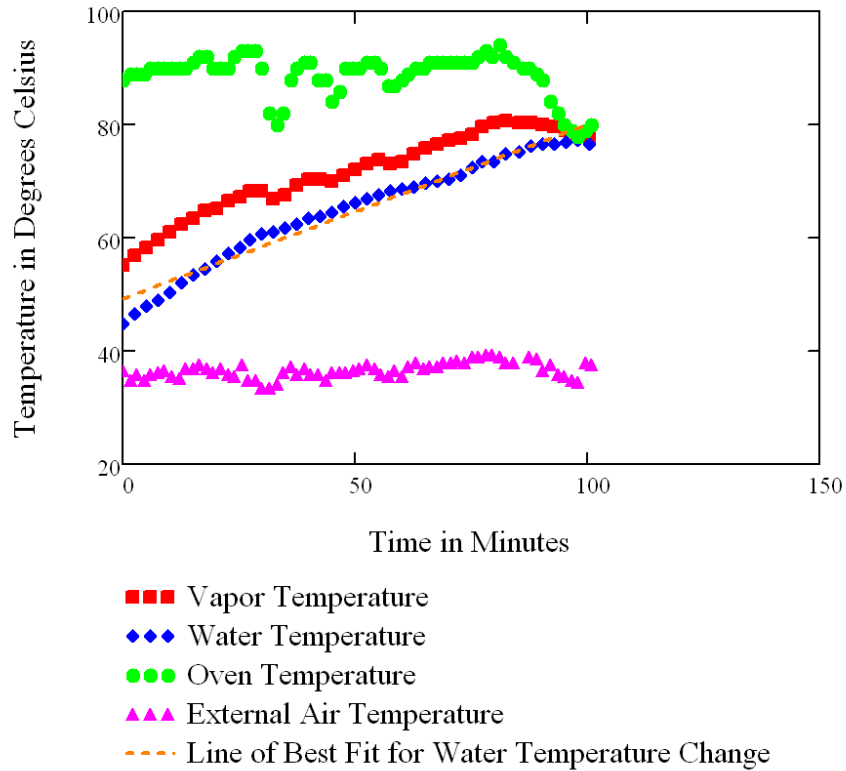


Figure 7: Increase in Temperature of Solar Autoclave Components Over Time. The temperatures of the water and vapor inside the pressure cooker, the air temperature internal to the oven, and the ambient air temperature were recorded over a period of approximately 100 minutes. The oven remained at a fairly constant average temperature over the time range; however, it shows large fluctuations due to short periods of cloud cover. The water temperature increased steadily throughout the measurement period.

The pressure cooker’s heating rate should be the same as that of the water. The heating rate of the pressure cooker and water, in combination with their masses and specific heats, were used in Equation 13 to determine the net power absorption of the autoclave. Because the oven air and water vapor had an insignificant mass and specific heat, and the autoclave insulation did not, on average, increase in temperature, their contributions were not factored into the autoclave’s calculated net power absorption.

The uncertainty inherent in the net power absorption was calculated through the propagation of uncertainty method, incorporating the uncertainty in $\frac{dT_{water}}{dt}$ calculated through the use of Equations 14 through 16 in MathCAD. The value of $\frac{dT_{water}}{dt}$ is shown in Figure 6; it is the slope of the dashed orange line. The net power absorption of the autoclave was thereby calculated at 29.9 ± 2.7 W, significantly smaller than the desired power absorption rate, 88.1 ± 21 W.

4.2. Examination of Model Validity

The power theoretically absorbable by the solar autoclave was approximated to be 127.7 ± 8.2 W using Equations 1 and 2. The difference between this total power input and the net power input of the system is 97.8 ± 6.3 W, corresponding almost exactly to the power loss

estimated through use of the thermodynamic heat conduction model described in the background. Expected heat loss was modeled, according to equations 9 through 11, at 94.88 ± 33 W. The fact that both the experimentally determined and theoretically modeled heat loss fall within each others' 95% confidence range suggests the model used for characterizing heat loss is accurate enough to be used for inferring methods for design improvements.

Additional confidence in the thermal model was obtained from the results of the follow-up experiment examining heat conductivity of small air gaps. The thermal model for the autoclave relied on the assumption that air convection between the autoclave's panes of glass was insignificant. Therefore, the heat conduction constant for air was used to model the thermal resistivity of the autoclave's air gap.

In the air gap experiment, one ice cube required 133.7 ± 0.02 minutes to melt. Its mass was determined after melting to be 15 ± 1 mL. The average ambient air temperature measured 25.2 ± 1.1 °C, while the average temperature of the small jar's inner surface was 5.0 ± 0.5 ° C. The air gap measured 15 ± 0.05 mm. Based on these values, the heat conduction coefficient of air in the gap was calculated at 0.03 ± 0.008 W/mK, using Equations 20 and 21. This value contains with 95% confidence the accepted conduction coefficient for air, 0.024 W/mK, indicating the presence of convective effects in gaps sized 15 mm and smaller are indeed insignificant.

4.3. Current Modes of Heat Loss and Implications for Future Designs

With the aid of Equations 9 through 11, it was possible to determine the heat loss separately through the top, bottom, and sides of the autoclave. The power loss from the top was modeled at 0.667 ± 0.05 W, while the power loss from the sides and bottom of the autoclave were modeled at 59.7 ± 12.7 W and 34.4 ± 12.4 W, respectively. The power loss through the top surprisingly accounts for only 1% of loss, while power loss through the sides accounts for fully 63% of the total, shown in Figure 8.

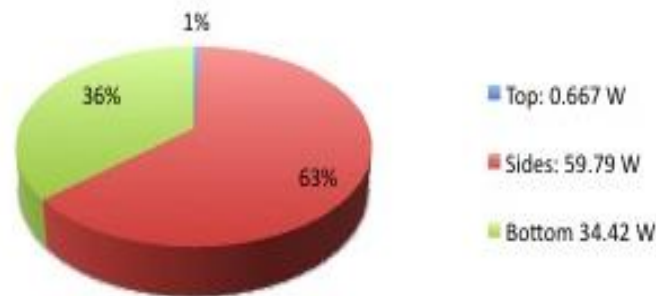


Figure 8: Heat Loss Through Autoclave Surfaces. According to the thermal model described in Equations 9 through 11, it is possible to determine the contribution of each autoclave surface to the total power loss. Surprisingly, heat loss through the top accounts for only 1% of the total, while the majority of the heat loss, 63%, is through the sides.

The net energy input of the system required to attain the desired heating rate was calculated according to Equations 14 and 15 to be 88.1 ± 21 W. This required net heat input is approximately 60% higher system's current power absorption. To achieve this power input, it

would be necessary to substantially improve the system's insulation and heat absorption capabilities. The modes of heat loss determined here suggest that replacing more of the system with double-paned glass could be helpful, as would decreasing the necessary area of insulation and thermal mass of the system. Additionally, it would be helpful to increase the area used to absorb solar energy. Another simple solution would be to widen and flatten the solar autoclave, thus increasing the energy absorption area while reducing heat loss through the sides. This method alone could increase the power absorption to that desired for sterilization.

4.4. Experimental Discrepancies, Limitations, and Accomplishments

The results obtained for overall heat absorption and loss are somewhat surprising given that, in less than two hours, it is possible to cook a good lunch in a similar solar cooker. Based on this fact alone, one might expect the heat absorption rate for the solar oven system to be substantially higher. However, it is likely that the lunches cooked in similar cookers, which often contain little water, have a substantially smaller heat capacity than the system described here. This may account for the lunches' reduced heating time and reliable cooking output.

In order to more precisely determine the quantity and locations of the autoclave's heat loss, it would be necessary not only to carry out the experiment over a larger temperature range, but also to improve the thermodynamic model through further specifications. Uncertainty in the values obtained for power input, output, and absorption is created primarily through use of the simplifying assumptions described previously. These simplifying assumptions make it difficult to determine whether detailed aspects of the solar autoclave's construction and setup, such as the positioning of the pressure cooker or the use of pine supports in the oven frame, significantly increase heat loss. In addition, since the temperatures of various autoclave surfaces were not explicitly measured, it is impossible to determine the exact contribution of radiant heat to the autoclave's total power losses.

The calculated results do, however, answer the key question of how much solar radiation a current model of solar powered autoclave is able to absorb; they also help determine the locations and ways in which the system loses power. From the measured results, it is clear that the solar autoclave loses a substantial amount of power, primarily through conduction, and that a few specific design changes may be enacted to bring the autoclave to desired sterilization standards. Satisfactory confidence in the overall thermal model suggests future design changes may be reliably chosen based on experimental results.

4.5. Measurements of Autoclave Materials

The following spatial measurements were taken of materials inside the solar cooker. The areas and thicknesses of each material were used to model the autoclave's heat transfer rates. The uncertainty in all direct measurements is ± 0.1 cm. Measurements were recorded for each panel of visible material. Some thicknesses were impossible to measure. These were determined by subtracting known thicknesses from the total and via referencing the building instructions provided by Las Mujeres Solares.

Table 1: Direct Measurements of Solar Oven Components. The majority of the solar oven components were directly measured to the nearest tenth of a centimeter using a tape measure. The air gap between

the panes of glass along with the thickness of the sawdust layer were determined through subtraction of other thicknesses from the total thickness. Thicknesses of the fiber board interior, the glass panels, and the gauge of the galvanized steel were determined through referencing the building instructions provided by Las Mujeres Solares; uncertainty in these dimensions is unknown and was not included in the heat loss model's 95% precision uncertainty.

Material	Thickness (cm)	Top/Bottom (cm)	Front/Back Panels (cm)	Side Panels (cm)
Galvanized Steel (Inner)	0.0475	57.7 × 64.0	64.0 × 27.5	57.7 × 27.5
Insulating Fiber Board	0.635	57.7 × 64.0	64.0 × 27.5	57.7 × 27.5
Layer of Sawdust	5.18	76.5 × 78.5	78.5 × 37.0	76.5 × 37.0
Plywood	0.635	76.5 × 78.5	78.5 × 37.0	76.5 × 37.0
Galvanized Steel (Outer)	0.0475	76.5 × 78.5	78.5 × 37.0	76.5 × 37.0
Glass Panels	0.635	64.5 × 66.0	NA	NA
Air Layer Between Glass	0.887	64.5 × 66.0	NA	NA

The only directly measured mass that played a role in the autoclave's thermal mass was that of the pressure cooker, 1.81 ± 0.09 kg.

4.6. Measurements of Air Gap Experiment Materials

To determine the areas over which heat transfer occurred in the air gap experiment, the heights, outer diameters, and thicknesses of each jar were measured, along with the thickness of the paper stack used to elevate the small jar. These measurements are shown in Table 2. The error present in each distance measurement is ± 0.05 mm. To determine the mass of the ice that melted, the initial and final water volume were also determined. They measured 48 ± 1 mL and 63 ± 1 mL, respectively.

Table 2: Direct Measurements of Air Gap Experiment Materials. The two glass jars and the paper stack used in the air gap experiment were measured to the nearest 0.05 mm using a pair of Vernier calipers. The relevant dimensions are the height, outer diameter of each jar, and jar thickness.

Object	Height (mm)	Outer Diameter (mm)	Thickness (mm)
Small Jar	49.5	35.0	3.0
Large Jar	67.5	65.0	3.0
Paper Stack	3.0	NA	NA

5. Conclusions

The solar autoclave was able to successfully absorb a power input of 29.9 ± 2.7 W. Although it would have been theoretically possible to absorb up to 127.7 ± 8.2 W on the day tested, the autoclave lost 97.8 ± 8.3 W via heat transfer through the autoclave's insulation. Power loss was confidently within the range of that predicted via a thermal model, which estimated total power loss to be 94.88 ± 33 W. The model predicted a power loss of 0.667 ± 0.05 W through the top of the autoclave, with a power loss from the sides and bottom of 59.7 ± 12.7 W and 34.4 ± 12.4 W, respectively. These findings imply, in relation to experimental objectives, that the autoclave's heat absorption and retention capabilities would need to be improved by approximately 60% before the autoclave could be reliably used to sterilize medical instruments in the desired cycle time.

Future work should be done to determine the feasibility of a more optimal design for a solar autoclave, as well as thermodynamically model and test such a design over the entire range of necessary temperatures. Such research would require building a new autoclave prototype and testing under relatively constant and sunny conditions. Future experiments would ideally include more surface temperature measurements to more closely distinguish instances of heat loss through conduction as opposed to convection and radiation. Future tests should also directly measure the intensity of incident radiation as it varies with temperature and time. In addition, it would be interesting to witness visually the temperature gradient of several pressure cooker components. This could be done through the aid of an infrared camera, particularly one with the ability to record images or video.

Other smaller experiments may also contribute to the development of a reliably working, inexpensive autoclave for off-grid clinics. These include investigations of alternative heating methods such as fire, gas, or small amounts electricity capable of production by photovoltaic cells. For each heating method investigated, detailed calculations of power requirements and heat loss should be made, similar to those determined in this particular experiment.

Based on the results of this experiment, work will continue during the summer on further improving the autoclave's heat retention capabilities. In particular, various methods of insulation will be tested, such bubble wrap, PVC foam, and various widths of air gaps encased in glass. Investigations will also be made of more modular autoclave designs, ones which could be used to sterilize several loads of medical instruments at once. Such tests will be performed both at MIT and in Nicaragua, in conjunction with student research at the Universidad Nacional de Ingenieria. In later stages of testing, consumer research will also be performed to determine responses of rural medical personnel to different types of working autoclave designs.

Acknowledgements

Many thanks go to Anna Young, Jose Gomez-Marquez, and Katie Inman for investigations of appropriate pressure vessel design. Thanks also to Anna Young, Justin Sharp, and to Professor Guenther Klante and Onel of the Universidad Nacional de Ingenieria for assistance in making necessary measurements. General project support was provided by El Centro Solar, Amy Banzaert, and Jessica Huang. Many thanks are also owed to Dr. Hughey and Dr. So for invaluable advice in performing necessary measurements, as well as to Dr. So and Justin Sharp for explaining the thermodynamic models involved.

References

- ¹ “Sterilization Cycles.” <<http://consteril.com/index.php?pg=41>>. Accessed 5/14/2010.
- ² “How Do Solar Panels Work.” <<http://www.glrea.org/articles/howDoSolarPanelsWork.html>>. Accessed 5/14/2010.
- ³ “Convective Heat Transfer.” <http://www.engineeringtoolbox.com/convective-heat-transfer-d_430.html>. Accessed 5/14/2010.
- ⁴ “Thermal Conductivity.” <http://www.engineeringtoolbox.com/thermal-conductivity-d_429.html>. Accessed 5/14/2010.
- ⁵ “Latent Heat” <http://www.engineeringtoolbox.com/fluids-evaporation-latent-heat-d_147.html>. Accessed 5/14/2010.
- ⁶ <<http://www.amazon.com/Military-Field-Style-Surgical-Instrument/dp/B000RGYEW>>. Accessed 5/14/2010.
- ⁷ <<http://www.amazon.com/Presto-6-Quart-Stainless-Pressure-Cooker/dp/B00006ISG6>>. Accessed 5/14/2010.
- ⁸ “Cooking with Pressure Cookers” <<http://missvickie.com/library/2ndgeneration.html>>. Accessed 5/14/2010.
- ⁹ “Specific Heat.” <http://www.engineeringtoolbox.com/specific-heat-metals-d_152.html>. Accessed 5/14/2010.
- ¹⁰ Colavito, C.J., “Solar Box Cooker Construction Manual”, Grupo Fenix, July, 2008 (unpublished).
- ¹¹ “Heat of Fusion.” <http://www.engineeringtoolbox.com/latent-heat-melting-solids-d_96.html>. Accessed 5/14/10.

Appendix A

The following thermodynamic constants were used in modeling the heat transfer properties of the autoclave and air gap experiment setup. These include the thermal conductivities of each material (Table 3), convection constants for each fluid/solid interface (Table 4), and specific heat capacities of heat absorbing modeled materials (Table 5).

Table 3: Thermal Conductivities of Solar Autoclave Materials. Standard thermal conductivities for materials used in the autoclave's construction were used to determine the resistivity in each layer of its insulation. Uncertainties for these values are not included in calculations, since they were referenced from standard values.

Material	Thermal Conductivity (W/mK)
Galvanized Steel	54
Fiberboard	0.048
Fine Sawdust	0.08
Plywood	0.13
Glass	1.05
Air	0.024

Table 4: Convection Constants Used. Approximate values of thermal convection constants were used to calculate thermal resistivities of fluid/solid boundaries in the autoclave and air gap experiment. The value of air with ground level wind speed was used for both the autoclave and air gap experiment. This is because the air gap experiment took place in a kitchen next to an opened back door; wind speed was estimated to be similar to that outside. The convection coefficient for air in a large closed container was used when modeling convection inside the solar oven. Uncertainties for the convection coefficient of air with typical ground level wind speed is approximated based on the reference cited and on estimated uncertainty in the wind speed around the autoclave. Uncertainty is not included for air in a large closed container, as the reference did not include a value for uncertainty.

Fluid	Convection Coefficient (W/m ² K)
Air (Typical Ground Level Wind Speed)	15 ± 5
Air (In Large Closed Container)	5

Table 5: Specific Heats of Solar Autoclave Materials. Standard specific heats for materials used in the autoclave's construction instrument sterilization were used to determine the heat absorption by the sterilization system. Uncertainties for these values are not included in calculations, since they were referenced from standard values.

Material	Specific Heat (J/kgK)
----------	-----------------------

Stainless Steel	500
Aluminum	940
Water	4,181
Steam	2080

MIT OpenCourseWare
<http://ocw.mit.edu>

21W.732 / ESG.21W732 Science Writing and New Media
Fall 2010

For information about citing these materials or our Terms of Use, visit: <http://ocw.mit.edu/terms>.